JACS
JOURNAL OF THE AMERICAN CHEMICAL SOCIETY

pubs.acs.org/JACS
Communication

Surface-Originated Weak Confinement in Tetrahedral Indium Arsenide Quantum Dots

Meeree Kim, Junho Lee, Jaegwan Jung, Daekwon Shin, Jugyoung Kim, Eunhye Cho, Yaolong Xing, Hyeonjun Jeong, Seongmin Park, Sang Ho Oh, Yong-Hyun Kim,* and Sohee Jeong*

Cite This: https://doi.org/10.1021/jacs.4c00966

ABSTRACT: While the shape-dependent quantum confinement (QC) effect in anisotropic semiconductor nanocrystals has been extensively studied, the QC in facet-specified polyhedral quantum dots (QDs) remains underexplored. Recently, tetrahedral nanocrystals have gained prominence in III−V nanocrystal synthesis. In our study, we successfully synthesized well-faceted tetrahedral InAs QDs with a first excitonic absorption extending up to 1700 nm. We observed an unconventional sizing curve, indicating weaker confinement than for equivalently volumed spherical QDs. The (111) surface states of InAs QDs persist at the conduction band minimum state even after ligand passivation with a significantly reduced band gap, which places tetrahedral QDs at lower energies in the sizing curve. Consequently, films composed of tetrahedral QDs demonstrate an extended photoresponse into the short-wave infrared region, compared to isovolume spherical QD films.

Colloidal quantum dots (QDs), semiconductor nanomaterials extensively studied for the past four decades, became a focal point following the discovery of size-dependent photophysical properties in a quantum confinement (QC) regime by Brus et al.[1] Over this period, the unique shape effect on spatially confined charges and excitons in anisotropic nanocrystals (NCs; e.g., rods and platelets), strong Coulomb interactions enhanced by dielectric confinement,[2] has been extensively investigated through describing quantitative parameters such as the sizing curve, molar absorption coefficient, and absorption cross-section.[3] However, the shape effect in QDs remains underexplored, and theoretical frameworks often adopt the assumption of a spherical geometry for QDs to understand their optoelectronic features better. Consequently, questions persist regarding a comprehensive understanding of their faceted shape effect on electronic structures in the QC regime.

Recently, a nonspherical, tetrahedral shape has gained prominence in zinc-blende QDs. III−V QDs are particularly notable due to the prevalence of a largely stable (111) facet in the halide-amine copassivation synthesis,[4,5] in addition to the unstable (100) facet compared to II−VI materials, which hinders the formation of other shapes such as platelets or cubes.[6,7] Considering the large exciton Bohr radius of InAs or InSb, which allows for technically observable shape evolution in large sizes within the QC regime,[8] these materials stand out as prime candidates to explore how faceted shapes differ from their spherical counterparts.

Herein, we have successfully synthesized well-faceted tetrahedral InAs QDs with a first excitonic absorption up to approximately 1700 nm and reported a sizing curve specifically for tetrahedral morphology, which has not been reported so far. By modifying our previous synthesis strategy for halide-amine-capped tetrahedral InP QDs, we achieved a finely edged tetrahedral shape with distinct excitonic peaks in the absorption spectra. This was accomplished by regulating the precursor reactivity through the suppression of transamination and varying precursor concentrations. Very interestingly, the sizing curve of tetrahedral InAs QDs is positioned at a lower energy compared to the spherical QDs of the same volume, resulting from surface-originated quantum confinement. We further present the higher field-effect electron mobilities and larger relative permittivity in QD films as altering the geometry of the isovolume QDs.

The recent colloidal InAs nanocrystal synthesis can be categorized based on two precursor species: aminoarsines ($As(NR_2)_3$) and silylarsines ($As(SiR_3)_3$). The majority of silylarsine-based InAs QDs synthesized with carboxylic acids are considered as "spherical", even though the shape deviates from a sphere in some reports due to irregularities.[9,10] In this work, we chose tris-dimethylaminoarsine ($As(NMe_2)_3$) as an As source since various shapes such as tetrahedrons and tetrapods have been reported with this classification of precursors in amine or phosphine ligands due to the significantly stabilized (111) surface by halide/amine copassivation.[11−13] The crystal shape diversity was obtained with a minor modification of the synthesis by Srivastava et al.:[14] a typical hot-injection step with lithium bis(trimethylsilyl)amide (LiHMDS) additives followed by the injection of reducing agent (diisobutyl aluminumhydride, DIBAL-H) (Figure 1a). To get various sized tetrahedral InAs QDs without forming alloying with phosphorus atoms, a hydride-based and mild

Received: January 20, 2024
Revised: March 14, 2024
Accepted: April 4, 2024

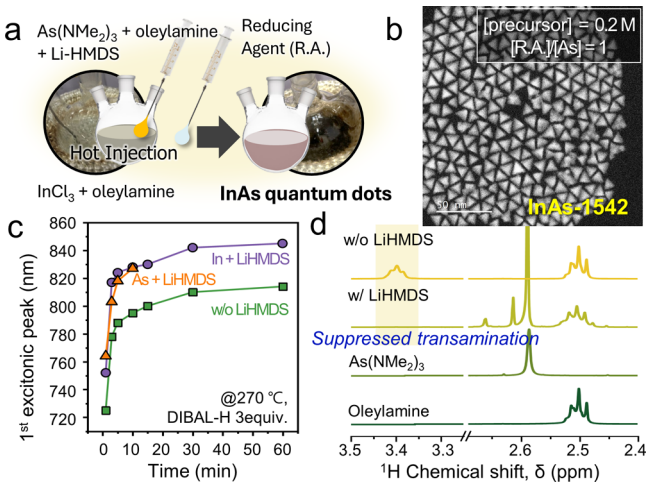

Figure 1. (a) Schematic illustration of tetrahedral InAs QD synthesis with a mild reducing agent and Li-HMDS. (b) HAADF-STEM image of tetrahedral InAs QDs. (c) 1st excitonic peak shift during InAs QD growth with and without 0.02 equiv of Li-HMDS additives. (d) ^{1}H NMR spectra of the As stock solution in *d*-toluene showing suppressed transamination with a presence of Li-HMDS (δ = 3.40: transaminated, δ = 2.50: free oleylamine $-CH_2-N-$ protons).

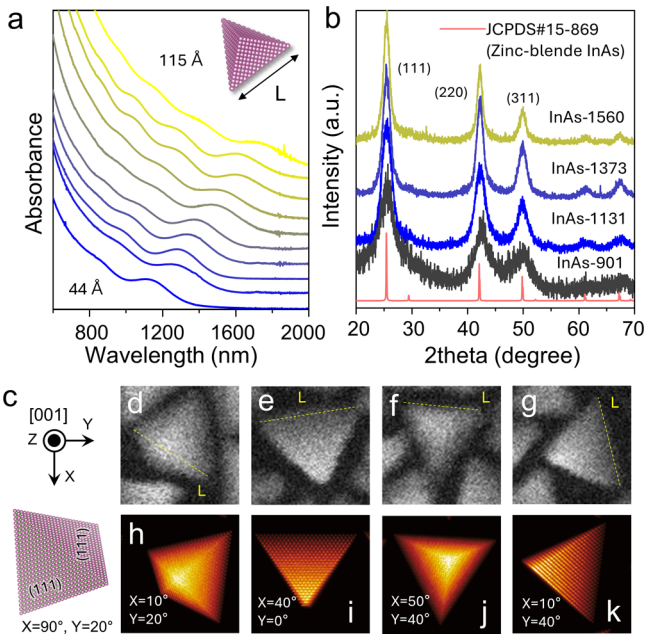

Figure 2. (a) Absorption spectra of tetrahedral InAs nanocrystals in various sizes of edge length (L) from 4.4 ± 0.6 to 11.6 ± 1.1 nm (see size distribution and shapes in Figures S10 and S11). (b) XRD pattern of InAs NCs with reference peaks for zinc-blende InAs from the database (JCPDS No. 15-869). (c) Schematic illustration, (d–g) experimental, and (h–k) simulated STEM images of tetrahedral InAs QDs rotated along the *x*-/*y*-axes as noted. InAs-1603 is used for experimental images.

reducing agent, DIBAL-H, was selected instead of aminophosphines. Before screening the synthetic parameters for size-control of tetrahedral QDs, it is important to note that the fast nucleation leading to monomer depletion isolates tetrapod formation and stops growth toward tetrahedron.[15] To widen the size range of the final tetrahedral QDs, we mitigated reactivity by addition of LiHMDS when $As(NMe_2)_3$ is mixed with oleylamine (See Supporting Information Discussion 1A). In low amounts (0.02 equiv), LiHMDS inhibits transamination between oleylamine and dimethylamine of $As(NMe_2)_3$ as shown in the absence of transaminated oleylamine in ^{1}H nuclear magnetic resonance (NMR) spectra (Figures 1d and S2). This results in a slowdown in the reaction and contributes to the QD size enlargement (Figure 1c).

Building on our screening result, we obtained various crystal shapes of InAs NCs (see Supporting Information Discussion 1A) and corresponding absorption spectra (Figure S1b). The absorption feature is complemented by weak but clearly identifiable band-edge photoluminescence (Figure S4). Notably, tetrahedral QDs smaller than sizes of 1100 nm first excitonic absorption were not observed. The ill-shaped or largely truncated NCs are formed in small sizes, since the decrease in surface-to-volume ratio outweighs surface energy stabilization effect by ligands when the NC shrinks.[16] Tetrahedral InAs QDs are obtained in the absorption range from 1100 to 1700 nm under high monomer concentrations (Figure 2a). Within this size range, elevating monomer concentration led to formation of larger InAs tetrahedrons, characterized by well-faceted shapes (Figure S11) and distinct excitonic features, collected after purification (Supporting Information Discussion 1B). Compared with the simulated scanning transmission electron microscopy (STEM) images of tetrahedral QDs along with rotation, the contrast variation in the QD projected as tetragons or triangles in experimental high angle annular dark field (HAADF)-STEM images is well-matched (Figure 2c–k). Syntheses carried out at 0.78 equiv of DIBAL-H at 0.2 M [In] delivered even larger tetrahedral QDs (beyond 1800 nm), but they had a very broad size distribution (Figure S6). This size control was supplemented by an X-ray diffraction (XRD) pattern, revealing a line width narrowing as the size of InAs tetrahedrons increased, while maintaining the zinc-blende crystal structure across all sizes (Figure 2b). The InAs QDs are In-rich without incorporation of Li or Al, as confirmed by ICP-MS measurements (Table S1). ^{1}H NMR and X-ray photoelectron spectroscopy (XPS) results support the idea that the QD surface is passivated with oleylamine/chloride ligands without oxidation (Figures S7 and S8).

The size of tetrahedral QDs has been reported as the edge length or the height of the projected triangle in TEM images.[4,11] Since tetrahedral QDs are also projected as tetragons depending on the rotation angle, we believe that the height measurement hinders the best description of the QD volume. The finely edged shape in this work enables measurement of the edge length (L) of QDs considering each projected angle (Supporting Information Discussion 2B). We therefore determined the sizing curve of tetrahedral InAs QDs as follows: the first excitonic peak positions (optical band gaps) are plotted against their corresponding average volume (Figure 3). QD volumes were calculated from the edge length as $V = L^3/(6\sqrt{2})$, while the peak positions of the lowest energy absorption transition were extracted from the second derivatives of the absorption spectra. A simple empirical fit equation adjusts the bulk InAs band gap (0.35 eV) for the size-dependent QC by correlating the energy of the first excitonic transition (E_g) with the QD volume (V_{QD}, nm^3) (Table S2).[17,18]

$$E_g(\text{eV}) = \frac{a}{V_{QD}^{\ c}} + 0.35$$

https://doi.org/10.1021/jacs.4c00966
J. Am. Chem. Soc. XXXX, XXX, XXX−XXX

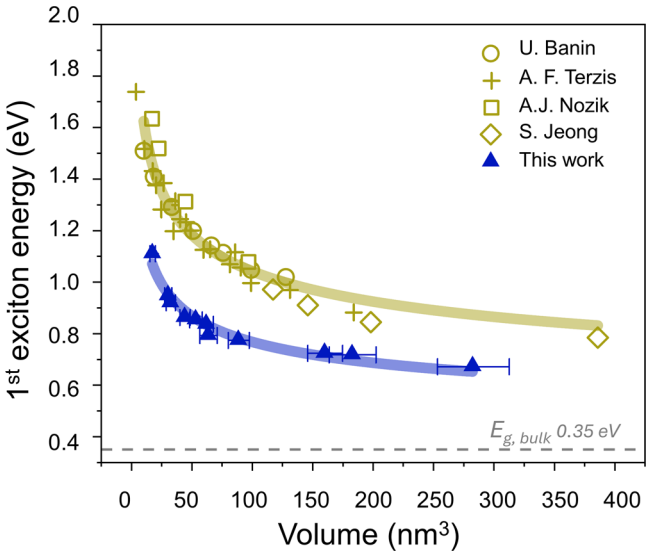

Figure 3. Size dependence of the first exciton energy (E_g) of tetrahedral and spherical InAs QDs, showing our own experimental data and experimental results from previous works for spherical QDs. Blue and yellowish-green lines are fitted to tetrahedral and spherical InAs QDs, respectively.[9,10,17−19] Reproduced with permission from refs 10, 17, and 18. Copyright 2021 Springer Nature. Copyright 1998 AIP Publishing. Copyright 2006 AIP Publishing.

Clearly, the sizing curve of tetrahedral InAs QDs is in lower E_g when compared to that of spherical shapes reported in previous literature.[9,10,19−21] This implies unconventionally weaker confinement of the tetrahedron. At first glance, this might appear to contradict the common notion that tetrahedrons should have higher confinement energy according to the particle-in-a-box (PIB) model.[22,23] Considering that the opposite trend is evident in InP QDs despite sharing the same tetrahedral geometry (Figure S12),[18,24,25] our observation in InAs QDs raises questions regarding potential additional factors influencing the electronic structure in the QC regime. We find that factors such as ligand type, surface-dependent electron effective mass, and exciton binding energy cannot fully offer valid explanations (Supporting Information Discussion 3).

The significant difference in surface characteristics between tetrahedral QDs and spherical shapes is the exclusive presence of the (111) facet in the tetrahedron. To understand how the (111) facet affects the electronic structure of tetrahedral QDs, we performed first-principles calculations for (100) and (111) surfaces passivated by acetic acid (AA) and chlorine/methylamine (MA), respectively.[4] While the bare (100) and (111) surfaces show metallic character with in-gap states due to dangling electrons at the surface (Figure 4a,c), the passivated (100) and (111) surfaces clear the in-gap states from the band gaps (Figure 4b,d). When the electronic structures of the passivated (100) surface are examined, the conduction band minimum (CBM) predominantly consists of the bulk state, as shown in Figure 4b(i), rendering the original bulk band gap almost unaffected by the ligand passivation, as shown in Figure 4a,b. In the case of the (111) surface, however, the bandgap is strongly influenced by surface passivation, resulting in a decreased band gap from 1.22 to 0.82 eV, representing a 33% reduction, as shown in Figure 4c,d.

This facet-dependent band gap reduction results from the difference in hybridization strength between the bulk CBM and the in-gap states under passivation of the metallic surface state by the ligands. The charge density of the in-gap state on the (100) surface is mostly localized on the surface before passivation and elevated above the bulk CBM after passivation, as shown in Figure 4a(ii),b(ii). In contrast, the lowest in-gap state at the bare (111) surface is distributed not only at the surface but also at the bulk region, as shown in Figure 4c(ii). The (111) in-gap state is significantly hybridized with the bulk CBM and persists even after passivation, as shown in Figure 4d(i,ii). The greater hybridization at the (111) surface is attributed to the absence of the surface reconstruction, unlikely with the passivated (100) surface. Therefore, QC excitonic states should be delocalized to all the (111) facets of tetrahedral QDs, resulting in weak QC of tetrahedral InAs QDs. This surface-originated CBM of the (111) surface likely reduces overlap with the VBM and, thus, optical transition rate, offering a possible explanation for their weaker optical transitions compared to the spherical InAs QDs. However, in the case of InP QDs, the (111) in-gap surface states exhibit less hybridization with the bulk CBM due to the larger band gap, as

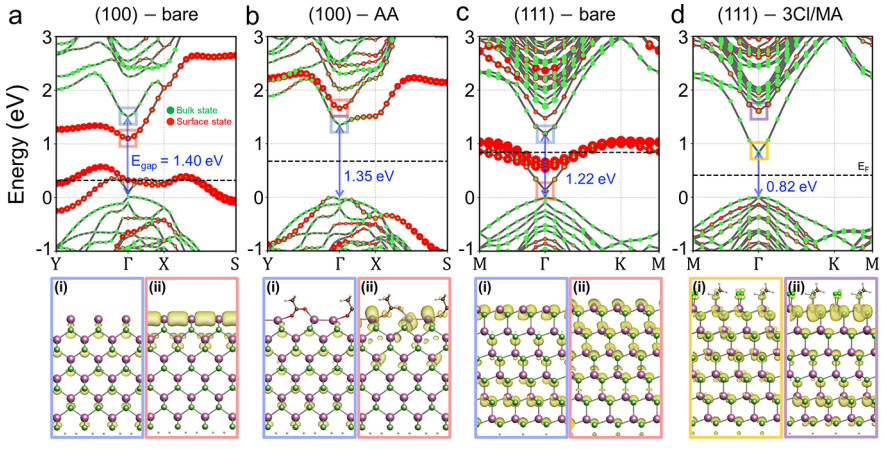

Figure 4. Site-decomposed electronic structures of (a) bare and (b) AA (acetic acid) passivated InAs (100) surfaces and (c) bare and (d) Cl/MA (methyl amine) copassivated InAs (111) surfaces (magenta: In, green: As, red: O, brown: C, lime: Cl, gray: N, and white: H). Insets (i) and (ii) show charge density profiles of the blue/red/orange/purple-squared states at the Γ-point. The bulk and surface states are projected from the indium of the middle layer and the surface of the slab model, respectively. The Fermi energy (E_F) is marked by the dashed black line in (a−d).

https://doi.org/10.1021/jacs.4c00966
J. Am. Chem. Soc. XXXX, XXX, XXX−XXX

shown in Figure S14. So, tetrahedral InP QDs display relatively strong QC, determined by the bulk portion rather than surface effects (Supporting Information Discussion 3).

We now prepared tetrahedral and spherical InAs QDs of the same volume (32 nm^3), with a bandgap around 1300 and 900 nm, respectively, derived from the sizing curves in Figure 3. The tetrahedral InAs QD films exhibited field-effect transistor (FET) electron mobility of 1.4×10^{-3} $cm^2/(V\ s)$ while the spherical one showed 1.2×10^{-4} $cm^2/(V\ s)$ (Figure S18). This observation is consistent with the previous results reported by Zhao et al.[25] about higher FET mobilities in tetrahedral InP NC films compared to the spherical one. The higher electron mobility of QD films can be explained by the larger volume fraction of inorganic core in QDs within the assembled films, which is determined by the volume of the QDs, interparticle distance, arrangement pattern, and packing density of QD assembly.[26,27] Both QDs are randomly assembled in the film, as confirmed by grazing incidence small-angle X-ray scattering (GISAXS) patterns (Figure S21). Considering the center-to-center distance (d_q) extracted from horizontal line-cuts, the estimated volume fraction is 57.2 and 31.2% for tetrahedral and spherical QD films, respectively (Table S4). The large volume fraction of tetrahedral QDs can be further confirmed by the relative permittivity (dielectric functions, $\tilde{\varepsilon} = \varepsilon_1 + i\varepsilon_2$) extracted through spectroscopic ellipsometry (Figure S19). Tetrahedral QD films exhibit larger relative permittivity than spherical ones in the range of 400 to 1600 nm (Figure S20a,b). Furthermore, the reduced amplitude of the fitted imaginary part (ε_2) for tetrahedral InAs QD solid implies their weaker confinement nature (Figure S20c,d). Building upon the previous discussions which suggest that tetrahedral InAs QDs could utilize incident photons and transport charges efficiently within the assembled film, a short-wave infrared (SWIR) phototransistor is fabricated with tetrahedral InAs QDs of bandgap targeted at 1310 nm (Figure S22). The transfer and output characteristics show that the photocurrent increases as the illumination power increases (Figure S22c,d). It is notable that the maximum responsivity (R) of the device reached 20 A/W without much optimization in the device structure and surface treatment. V_g-dependent R tuning further expands its application potential.

Throughout this study, finely edged tetrahedral InAs QDs were synthesized, featuring distinct optical transitions up to 1700 nm. We highlighted an unconventional sizing curve for tetrahedral InAs QDs, located in the lower energy region compared to equivalently volumed spherical QDs. DFT analysis explained that the hybridization of (111) in-gap states with bulk CBM results in a reduced band gap, indicating a "surface-originated confinement effect" in addition to the QC from a bulk PIB model. This surface-originated QC is influenced by the small bandgap of InAs, and InP QDs exhibit opposite trends. The sizing curve was used for the fabrication of tetrahedral QD films with the same volume of spherical QDs, showing higher FET charge mobilities attributed to the large volume fraction of tetrahedral QDs within the films. Our findings provide new insight for understanding the quantum confinement effect in faceted QDs, particularly those of smaller band gap materials, while comprehensive correlation to the PIB model and achieving more monodispersed and arranged tetrahedral QDs will be areas of future study.

■ ASSOCIATED CONTENT

Supporting Information

The Supporting Information is available free of charge at https://pubs.acs.org/doi/10.1021/jacs.4c00966.

General information, synthetic procedures, and supplemental data (PDF)

■ AUTHOR INFORMATION

Corresponding Authors

Yong-Hyun Kim − *Department of Physics, Korea Advanced Institute of Science and Technology (KAIST), Daejeon 34141, Republic of Korea; School of Physics, Institute of Science, Suranaree University of Technology, Nakhon Ratchasima 30000, Thailand;* orcid.org/0000-0003-4255-2068; Email: yong.hyun.kim@kaist.ac.kr

Sohee Jeong − *Department of Energy Science (DOES) and Center for Artificial Atoms, Sungkyunkwan University (SKKU), Suwon 16419 Gyeonggi-do, Republic of Korea; Sungkyunkwan Institute of Energy Science and Technology (SIEST), Sungkyunkwan University (SKKU), Suwon 16419 Gyeonggi-do, Republic of Korea;* orcid.org/0000-0002-9863-1374; Email: s.jeong@skku.edu

Authors

Meeree Kim − *Department of Energy Science (DOES) and Center for Artificial Atoms, Sungkyunkwan University (SKKU), Suwon 16419 Gyeonggi-do, Republic of Korea;* orcid.org/0000-0001-9183-0517

Junho Lee − *Department of Physics, Korea Advanced Institute of Science and Technology (KAIST), Daejeon 34141, Republic of Korea*

Jaegwan Jung − *Department of Physics, Korea Advanced Institute of Science and Technology (KAIST), Daejeon 34141, Republic of Korea;* orcid.org/0009-0009-1310-0290

Daekwon Shin − *Department of Energy Science (DOES) and Center for Artificial Atoms, Sungkyunkwan University (SKKU), Suwon 16419 Gyeonggi-do, Republic of Korea*

Jugyoung Kim − *Department of Energy Science (DOES) and Center for Artificial Atoms, Sungkyunkwan University (SKKU), Suwon 16419 Gyeonggi-do, Republic of Korea*

Eunhye Cho − *Department of Energy Science (DOES) and Center for Artificial Atoms, Sungkyunkwan University (SKKU), Suwon 16419 Gyeonggi-do, Republic of Korea*

Yaolong Xing − *Department of Energy Engineering, KENTECH Institute for Energy Materials and Devices, Korea Institute of Energy Technology (KENTECH), Naju-si 58330 Jeonnam, Republic of Korea*

Hyeonjun Jeong − *Department of Energy Science (DOES) and Center for Artificial Atoms, Sungkyunkwan University (SKKU), Suwon 16419 Gyeonggi-do, Republic of Korea*

Seongmin Park − *Department of Energy Science (DOES) and Center for Artificial Atoms, Sungkyunkwan University (SKKU), Suwon 16419 Gyeonggi-do, Republic of Korea*

Sang Ho Oh − *Department of Energy Engineering, KENTECH Institute for Energy Materials and Devices, Korea Institute of Energy Technology (KENTECH), Naju-si 58330 Jeonnam, Republic of Korea*

Complete contact information is available at: https://pubs.acs.org/10.1021/jacs.4c00966

https://doi.org/10.1021/jacs.4c00966
J. Am. Chem. Soc. XXXX, XXX, XXX−XXX

Notes

The authors declare no competing financial interest.

■ ACKNOWLEDGMENTS

This research was supported by the Creative Materials Discovery Program through the National Research Foundation (NRF) of Korea (NRF-2019M3D1A1078299, NRF-2019M3D1A1078302) and an NRF grant funded by the MSIT (NRF-2022M3H4A1A03076626, NRF-2022R1A2C2091486). This research was also supported by Grant RS-2022-00144108 funded by the Ministry of Trade, Industry and Energy of the Korean government. This research was supported by the SungKyunKwan University and the BK21 FOUR(Graduate School Innovation) funded by the Ministry of Education (MOE, Korea) and National Research Foundation of Korea (NRF). M.K. is supported by Basic Science Research Program through the NRF of Korea funded by the Ministry of Education (2022R1A6A3A0108754111).

■ REFERENCES

(1) Brus, L. E. Electron−electron and electron-hole interactions in small semiconductor crystallites: The size dependence of the lowest excited electronic state. *J. Chem. Phys.* **1984**, *80*, 4403.

(2) (a) Peng, X.; Manna, L.; Yang, W.; Wickham, J.; Scher, E.; Kadavanich, A.; Alivisatos, A. P. Shape control of CdSe nanocrystals. *Nature* **2000**, *404*, 59. (b) Shabaev, A.; Efros, A. L. 1D Exciton Spectroscopy of Semiconductor Nanorods. *Nano Lett.* **2004**, *4*, 1821. (c) Katz, D.; Wizansky, T.; Millo, O.; Rothenberg, E.; Mokari, T.; Banin, U. Size-Dependent Tunneling and Optical Spectroscopy of CdSe Quantum Rods. *Phys. Rev. Lett.* **2002**, *89*, 086801. (d) Ithurria, S.; Dubertret, B. Quasi 2D Colloidal CdSe Platelets with Thicknesses Controlled at the Atomic Level. *J. Am. Chem. Soc.* **2008**, *130*, 16504. (e) Lhuillier, E.; Pedetti, S.; Ithurria, S.; Nadal, B.; Heuclin, H.; Dubertret, B. Two-Dimensional Colloidal Metal Chalcogenides Semiconductors: Synthesis, Spectroscopy, and Applications. *Acc. Chem. Res.* **2015**, *48*, 22.

(3) (a) Efros, A. L.; Brus, L. E. Nanocrystal Quantum Dots: From Discovery to Modern Development. *ACS Nano* **2021**, *15*, 6192. (b) Ithurria, S.; Tessier, M. D.; Mahler, B.; Lobo, R. P. S. M.; Dubertret, B.; Efros, A. L. Colloidal nanoplatelets with two-dimensional electronic structure. *Nat. Mater.* **2011**, *10*, 936. (c) Movilla, J. L.; Planelles, J.; Climente, J. I. Dielectric Confinement Enables Molecular Coupling in Stacked Colloidal Nanoplatelets. *J. Phys. Chem. Lett.* **2020**, *11*, 3294. (d) Taguchi, S.; Saruyama, M.; Teranishi, T.; Kanemitsu, Y. Quantized Auger recombination of biexcitons in CdSe nanorods studied by time-resolved photo-luminescence and transient-absorption spectroscopy. *Phys. Rev. B* **2011**, *83*, 155324.

(4) Kim, K.; Yoo, D.; Choi, H.; Tamang, S.; Ko, J.-H.; Kim, S.; Kim, Y.-H.; Jeong, S. Halide−Amine Co-Passivated Indium Phosphide Colloidal Quantum Dots in Tetrahedral Shape. *Angew. Chem., Int. Ed.* **2016**, *55*, 3714.

(5) Ko, J.-H.; Yoo, D.; Kim, Y.-H. Atomic models for anionic ligand passivation of cation-rich surfaces of IV−VI, II−VI, and III−V colloidal quantum dots. *Chem. Commun.* **2017**, *53*, 388.

(6) Dümbgen, K. C.; Zito, J.; Infante, I.; Hens, Z. Shape, Electronic Structure, and Trap States in Indium Phosphide Quantum Dots. *Chem. Mater.* **2021**, *33*, 6885.

(7) Kim, T.; Shin, D.; Kim, M.; Kim, H.; Cho, E.; Choi, M.; Kim, J.; Jang, E.; Jeong, S. Development of Group III−V Colloidal Quantum Dots for Optoelectronic Applications. *ACS Energy Lett.* **2023**, *8*, 447.

(8) Kim, M.; Choi, M.; Choi, S.; Jeong, S. Semiconductor Nanocrystals: Unveiling the Chemistry behind Different Facets. *Acc. Chem. Res.* **2023**, *56*, 1756.

(9) Tamang, S.; Lee, S.; Choi, H.; Jeong, S. Tuning Size and Size Distribution of Colloidal InAs Nanocrystals via Continuous Supply of Prenucleation Clusters on Nanocrystal Seeds. *Chem. Mater.* **2016**, *28*, 8119.

(10) Kim, T.; Park, S.; Jeong, S. Diffusion dynamics controlled colloidal synthesis of highly monodisperse InAs nanocrystals. *Nat. Commun.* **2021**, *12*, 3013.

(11) Leemans, J.; Respekta, D.; Bai, J.; Braeuer, S.; Vanhaecke, F.; Hens, Z. Formation of Colloidal In(As,P) Quantum Dots Active in the Short-Wave Infrared, Promoting Growth through Temperature Ramps. *ACS Nano* **2023**, *17*, 20002.

(12) Kim, S.; Park, S.; Kim, M.; Jeong, S. Synthesis of single-crystalline InP tetrapod nanocrystals via addition of $ZnCl_2$. *Bull. Korean Chem. Soc.* **2023**, *44*, 483.

(13) Liu, Z.; Pascazio, R.; Goldoni, L.; Maggioni, D.; Zhu, D.; Ivanov, Y. P.; Divitini, G.; Camarelles, J. L.; Jalali, H. B.; Infante, I.; et al. Colloidal InAs Tetrapods: Impact of Surfactants on the Shape Control. *J. Am. Chem. Soc.* **2023**, *145*, 18329.

(14) Srivastava, V.; Janke, E. M.; Diroll, B. T.; Schaller, R. D.; Talapin, D. V. Facile, Economic and Size-Tunable Synthesis of Metal Arsenide Nanocrystals. *Chem. Mater.* **2016**, *28*, 6797.

(15) Kim, Y.; Choi, H.; Lee, Y.; Koh, W.-k.; Cho, E.; Kim, T.; Kim, H.; Kim, Y.-H.; Jeong, H. Y.; Jeong, S. Tailored growth of single-crystalline InP tetrapods. *Nat. Commun.* **2021**, *12*, 4454.

(16) Lee, H.; Yoon, D.-E.; Koh, S.; Kang, M. S.; Lim, J.; Lee, D. C. Ligands as a universal molecular toolkit in synthesis and assembly of semiconductor nanocrystals. *Chem. Sci.* **2020**, *11*, 2318.

(17) (a) Narayanaswamy, A.; Feiner, L. F.; Meijerink, A.; van der Zaag, P. J. The Effect of Temperature and Dot Size on the Spectral Properties of Colloidal InP/ZnS Core−Shell Quantum Dots. *ACS Nano* **2009**, *3*, 2539. (b) Fu, H.; Zunger, A. InP quantum dots: Electronic structure, surface effects, and the redshifted emission. *Phys. Rev. B* **1997**, *56*, 1496. (c) Fu, H.; Zunger, A. Local-density-derived semiempirical nonlocal pseudopotentials for InP with applications to large quantum dots. *Phys. Rev. B* **1997**, *55*, 1642.

(18) Cho, E.; Jang, H.; Lee, J.; Jang, E. Modeling on the size dependent properties of InP quantum dots: a hybrid functional study. *Nanotechnology* **2013**, *24*, 215201.

(19) Banin, U.; Lee, C. J.; Guzelian, A. A.; Kadavanich, A. V.; Alivisatos, A. P.; Jaskolski, W.; Bryant, G. W.; Efros, A. L.; Rosen, M. Size-dependent electronic level structure of InAs nanocrystal quantum dots: Test of multiband effective mass theory. *J. Chem. Phys.* **1998**, *109*, 2306.

(20) Baskoutas, S.; Terzis, A. F. Size-dependent band gap of colloidal quantum dots. *J. Appl. Phys.* **2006**, *99*, 013708.

(21) Yu, P.; Zhu, K.; Norman, A. G.; Ferrere, S.; Frank, A. J.; Nozik, A. J. Nanocrystalline TiO2 Solar Cells Sensitized with InAs Quantum Dots. *J. Phys. Chem. B* **2006**, *110*, 25451.

(22) Turner, J. W. On the quantum particle in a polyhedral box. *J. Phys. A: Math. Gen.* **1984**, *17*, 2791.

(23) Li, W.-K.; Blinder, S. M. Variational solution for particle in a regular tetrahedron. *Chem. Phys. Lett.* **2010**, *496*, 339.

(24) (a) Kim, K.; Han, C.-S.; Jeong, S. Design and synthesis of photostable multi-shell Cd-free nanocrystal quantum dots for LED applications. *J. Mater. Chem.* **2012**, *22*, 21370. (b) Crisp, R. W.; Kirkwood, N.; Grimaldi, G.; Kinge, S.; Siebbeles, L. D. A.; Houtepen, A. J. Highly Photoconductive InP Quantum Dots Films and Solar Cells. *ACS Appl. Energy Mater.* **2018**, *1*, 6569. (c) Almeida, G.; van der Poll, L.; Evers, W. H.; Szoboszlai, E.; Vonk, S. J. W.; Rabouw, F. T.; Houtepen, A. J. Size-Dependent Optical Properties of InP Colloidal Quantum Dots. *Nano Lett.* **2023**, *23*, 8697.

(25) Zhao, T.; Zhao, Q.; Lee, J.; Yang, S.; Wang, H.; Chuang, M.-Y.; He, Y.; Thompson, S. M.; Liu, G.; Oh, N.; et al. Engineering the Surface Chemistry of Colloidal InP Quantum Dots for Charge Transport. *Chem. Mater.* **2022**, *34*, 8306.

(26) Chehaibou, B.; Izquierdo, E.; Chu, A.; Abadie, C.; Cavallo, M.; Khalili, A.; Dang, T. H.; Gréboval, C.; Xu, X. Z.; Ithurria, S.; et al. The complex optical index of PbS nanocrystal thin films and their use for short wave infrared sensor design. *Nanoscale* **2022**, *14*, 2711.

(27) Shin, D.; Park, Y.; Jeong, H.; Tran, H.-C. V.; Jang, E.; Jeong, S. Exploring the Potential of Colloidal Quantum Dots for Near-Infrared

https://doi.org/10.1021/jacs.4c00966
J. Am. Chem. Soc. XXXX, XXX, XXX−XXX

to Short-Wavelength Infrared Applications. *Adv. Energy Mater.* **2024**, 2304550.

https://doi.org/10.1021/jacs.4c00966
J. Am. Chem. Soc. XXXX, XXX, XXX−XXX